Search for the Radiative Decays $B \to \rho\gamma$ and $B^0 \to \omega\gamma$

B. Aubert,[1] R. Barate,[1] D. Boutigny,[1] J.-M. Gaillard,[1] A. Hicheur,[1] Y. Karyotakis,[1] J. P. Lees,[1] P. Robbe,[1] V. Tisserand,[1] A. Zghiche,[1] A. Palano,[2] A. Pompili,[2] J. C. Chen,[3] N. D. Qi,[3] G. Rong,[3] P. Wang,[3] Y. S. Zhu,[3] G. Eigen,[4] I. Ofte,[4] B. Stugu,[4] G. S. Abrams,[5] A.W. Borgland,[5] A. B. Breon,[5] D. N. Brown,[5] J. Button-Shafer,[5] R. N. Cahn,[5] E. Charles,[5] C. T. Day,[5] M. S. Gill,[5] A.V. Gritsan,[5] Y. Groysman,[5] R. G. Jacobsen,[5] R.W. Kadel,[5] J. Kadyk,[5] L. T. Kerth,[5] Yu. G. Kolomensky,[5] J. F. Kral,[5] G. Kukartsev,[5] C. LeClerc,[5] M. E. Levi,[5] G. Lynch,[5] L. M. Mir,[5] P. J. Oddone,[5] T. J. Orimoto,[5] M. Pripstein,[5] N. A. Roe,[5] A. Romosan,[5] M.T. Ronan,[5] V. G. Shelkov,[5] A.V. Telnov,[5] W. A. Wenzel,[5] T. J. Harrison,[6] C. M. Hawkes,[6] D. J. Knowles,[6] R. C. Penny,[6] A. T. Watson,[6] N. K. Watson,[6] T. Deppermann,[7] K. Goetzen,[7] H. Koch,[7] B. Lewandowski,[7] M. Pelizaeus,[7] K. Peters,[7] H. Schmuecker,[7] M. Steinke,[7] N. R. Barlow,[8] W. Bhimji,[8] J. T. Boyd,[8] N. Chevalier,[8] W. N. Cottingham,[8] C. Mackay,[8] F. F. Wilson,[8] C. Hearty,[9] T. S. Mattison,[9] J. A. McKenna,[9] D. Thiessen,[9] P. Kyberd,[10] A. K. McKemey,[10] V. E. Blinov,[11] A. D. Bukin,[11] V. B. Golubev,[11] V. N. Ivanchenko,[11] E. A. Kravchenko,[11] A. P. Onuchin,[11] S. I. Serednyakov,[11] Yu. I. Skovpen,[11] E. P. Solodov,[11] A. N. Yushkov,[11] D. Best,[12] M. Chao,[12] D. Kirkby,[12] A. J. Lankford,[12] M. Mandelkern,[12] S. McMahon,[12] R. K. Mommsen,[12] W. Roethel,[12] D. P. Stoker,[12] C. Buchanan,[13] H. K. Hadavand,[14] E. J. Hill,[14] D. B. MacFarlane,[14] H. P. Paar,[14] Sh. Rahatlou,[14] U. Schwanke,[14] V. Sharma,[14] J.W. Berryhill,[15] C. Campagnari,[15] B. Dahmes,[15] N. Kuznetsova,[15] S. L. Levy,[15] O. Long,[15] A. Lu,[15] M. A. Mazur,[15] J. D. Richman,[15] W. Verkerke,[15] J. Beringer,[16] A. M. Eisner,[16] C. A. Heusch,[16] W. S. Lockman,[16] T. Schalk,[16] R. E. Schmitz,[16] B. A. Schumm,[16] A. Seiden,[16] M. Turri,[16] W. Walkowiak,[16] D. C. Williams,[16] M. G. Wilson,[16] J. Albert,[17] E. Chen,[17] M. P. Dorsten,[17] G. P. Dubois-Felsmann,[17] A. Dvoretskii,[17] D. G. Hitlin,[17] I. Narsky,[17] F. C. Porter,[17] A. Ryd,[17] A. Samuel,[17] S. Yang,[17] S. Jayatilleke,[18] G. Mancinelli,[18] B. T. Meadows,[18] M. D. Sokoloff,[18] T. Barillari,[19] F. Blanc,[19] P. Bloom,[19] P. J. Clark,[19] W. T. Ford,[19] U. Nauenberg,[19] A. Olivas,[19] P. Rankin,[19] J. Roy,[19] J. G. Smith,[19] W. C. van Hoek,[19] L. Zhang,[19] J. L. Harton,[20] T. Hu,[20] A. Soffer,[20] W. H. Toki,[20] R. J. Wilson,[20] J. Zhang,[20] D. Altenburg,[21] T. Brandt,[21] J. Brose,[21] T. Colberg,[21] M. Dickopp,[21] R. S. Dubitzky,[21] A. Hauke,[21] H. M. Lacker,[21] E. Maly,[21] R. Müller-Pfefferkorn,[21] R. Nogowski,[21] S. Otto,[21] K. R. Schubert,[21] R. Schwierz,[21] B. Spaan,[21] L. Wilden,[21] D. Bernard,[22] G. R. Bonneaud,[22] F. Brochard,[22] J. Cohen-Tanugi,[22] Ch. Thiebaux,[22] G. Vasileiadis,[22] M. Verderi,[22] A. Khan,[23] D. Lavin,[23] F. Muheim,[23] S. Playfer,[23] J. E. Swain,[23] J. Tinslay,[23] C. Bozzi,[24] L. Piemontese,[24] A. Sarti,[24] E. Treadwell,[25] F. Anulli,[26,*] R. Baldini-Ferroli,[26] A. Calcaterra,[26] R. de Sangro,[26] D. Falciai,[26] G. Finocchiaro,[26] P. Patteri,[26] I. M. Peruzzi,[26,*] M. Piccolo,[26] A. Zallo,[26] A. Buzzo,[27] R. Contri,[27] G. Crosetti,[27] M. Lo Vetere,[27] M. Macri,[27] M. R. Monge,[27] S. Passaggio,[27] F. C. Pastore,[27] C. Patrignani,[27] E. Robutti,[27] A. Santroni,[27] S. Tosi,[27] S. Bailey,[28] M. Morii,[28] M. L. Aspinwall,[29] D. A. Bowerman,[29] P. D. Dauncey,[29] U. Egede,[29] I. Eschrich,[29] G.W. Morton,[29] J. A. Nash,[29] P. Sanders,[29] G. P. Taylor,[29] G. J. Grenier,[30] S.-J. Lee,[30] U. Mallik,[30] J. Cochran,[31] H. B. Crawley,[31] J. Lamsa,[31] W. T. Meyer,[31] S. Prell,[31] E. I. Rosenberg,[31] J. Yi,[31] M. Davier,[32] G. Grosdidier,[32] A. Höcker,[32] S. Laplace,[32] F. Le Diberder,[32] V. Lepeltier,[32] A. M. Lutz,[32] T. C. Petersen,[32] S. Plaszczynski,[32] M. H. Schune,[32] L. Tantot,[32] G. Wormser,[32] R. M. Bionta,[33] V. Brigljević,[33] C. H. Cheng,[33] D. J. Lange,[33] D. M. Wright,[33] A. J. Bevan,[34] J. R. Fry,[34] E. Gabathuler,[34] R. Gamet,[34] M. Kay,[34] D. J. Payne,[34] R. J. Sloane,[34] C. Touramanis,[34] J. J. Back,[35] G. Bellodi,[35] P. F. Harrison,[35] H.W. Shorthouse,[35] P. Strother,[35] P. B. Vidal,[35] G. Cowan,[36] H. U. Flaecher,[36] S. George,[36] M. G. Green,[36] A. Kurup,[36] C. E. Marker,[36] T. R. McMahon,[36] S. Ricciardi,[36] F. Salvatore,[36] G. Vaitsas,[36] M. A. Winter,[36] D. Brown,[37] C. L. Davis,[37] J. Allison,[38] R. J. Barlow,[38] A. C. Forti,[38] P. A. Hart,[38] F. Jackson,[38] G. D. Lafferty,[38] A. J. Lyon,[38] J. H. Weatherall,[38] J. C. Williams,[38] A. Farbin,[39] A. Jawahery,[39] D. Kovalskyi,[39] C. K. Lae,[39] V. Lillard,[39] D. A. Roberts,[39] G. Blaylock,[40] C. Dallapiccola,[40] K. T. Flood,[40] S. S. Hertzbach,[40] R. Kofler,[40] V. B. Koptchev,[40] T. B. Moore,[40] H. Staengle,[40] S. Willocq,[40] R. Cowan,[41] G. Sciolla,[41] F. Taylor,[41] R. K. Yamamoto,[41] D. J. J. Mangeol,[42] M. Milek,[42] P. M. Patel,[42] A. Lazzaro,[43] F. Palombo,[43] J. M. Bauer,[44] L. Cremaldi,[44] V. Eschenburg,[44] R. Godang,[44] R. Kroeger,[44] J. Reidy,[44] D. A. Sanders,[44] D. J. Summers,[44] H.W. Zhao,[44] C. Hast,[45] P. Taras,[45] H. Nicholson,[46] C. Cartaro,[47] N. Cavallo,[47,†] G. De Nardo,[47] F. Fabozzi,[47,†] C. Gatto,[47] L. Lista,[47] P. Paolucci,[47] D. Piccolo,[47] C. Sciacca,[47] M. A. Baak,[48] G. Raven,[48] J. M. LoSecco,[49] T. A. Gabriel,[50] B. Brau,[51] T. Pulliam,[51] J. Brau,[52] R. Frey,[52] M. Iwasaki,[52] C. T. Potter,[52] N. B. Sinev,[52] D. Strom,[52] E. Torrence,[52] F. Colecchia,[53] A. Dorigo,[53] F. Galeazzi,[53] M. Margoni,[53] M. Morandin,[53] M. Posocco,[53] M. Rotondo,[53] F. Simonetto,[53] R. Stroili,[53] G. Tiozzo,[53] C. Voci,[53] M. Benayoun,[54] H. Briand,[54] J. Chauveau,[54] P. David,[54] Ch. de la Vaissière,[54] L. Del Buono,[54] O. Hamon,[54] Ph. Leruste,[54] J. Ocariz,[54] M. Pivk,[54] L. Roos,[54] J. Stark,[54] S. T'Jampens,[54] P. F. Manfredi,[55] V. Re,[55] L. Gladney,[56] Q. H. Guo,[56] J. Panetta,[56] C. Angelini,[57] G. Batignani,[57] S. Bettarini,[57] M. Bondioli,[57] F. Bucci,[57]

 0031-9007/04/92(11)/111801(7)$22.50

G. Calderini,[57] M. Carpinelli,[57] F. Forti,[57] M. A. Giorgi,[57] A. Lusiani,[57] G. Marchiori,[57] F. Martinez-Vidal,[57,‡] M. Morganti,[57] N. Neri,[57] E. Paoloni,[57] M. Rama,[57] G. Rizzo,[57] F. Sandrelli,[57] J. Walsh,[57] M. Haire,[58] D. Judd,[58] K. Paick,[58] D. E. Wagoner,[58] N. Danielson,[59] P. Elmer,[59] C. Lu,[59] V. Miftakov,[59] J. Olsen,[59] A. J. S. Smith,[59] E.W. Varnes,[59] F. Bellini,[60] G. Cavoto,[59,60] D. del Re,[60] R. Faccini,[14,60] F. Ferrarotto,[60] F. Ferroni,[60] M. Gaspero,[60] E. Leonardi,[60] M. A. Mazzoni,[60] S. Morganti,[60] M. Pierini,[60] G. Piredda,[60] F. Safai Tehrani,[60] M. Serra,[60] C. Voena,[60] S. Christ,[61] G. Wagner,[61] R. Waldi,[61] T. Adye,[62] N. De Groot,[62] B. Franek,[62] N. I. Geddes,[62] G. P. Gopal,[62] E. O. Olaiya,[62] S. M. Xella,[62] R. Aleksan,[63] S. Emery,[63] A. Gaidot,[63] S. F. Ganzhur,[63] P.-F. Giraud,[63] G. Hamel de Monchenault,[63] W. Kozanecki,[63] M. Langer,[63] G.W. London,[63] B. Mayer,[63] G. Schott,[63] G. Vasseur,[63] Ch. Yeche,[63] M. Zito,[63] M.V. Purohit,[64] A.W. Weidemann,[64] F. X. Yumiceva,[64] D. Aston,[65] R. Bartoldus,[65] N. Berger,[65] A. M. Boyarski,[65] O. L. Buchmueller,[65] M. R. Convery,[65] D. P. Coupal,[65] D. Dong,[65] J. Dorfan,[65] D. Dujmic,[65] W. Dunwoodie,[65] R. C. Field,[65] T. Glanzman,[65] S. J. Gowdy,[65] E. Grauges-Pous,[65] T. Hadig,[65] V. Halyo,[65] T. Hryn'ova,[65] W. R. Innes,[65] C. P. Jessop,[65] M. H. Kelsey,[65] P. Kim,[65] M. L. Kocian,[65] U. Langenegger,[65] D.W. G. S. Leith,[65] S. Luitz,[65] V. Luth,[65] H. L. Lynch,[65] H. Marsiske,[65] S. Menke,[65] R. Messner,[65] D. R. Muller,[65] C. P. O'Grady,[65] V. E. Ozcan,[65] A. Perazzo,[65] M. Perl,[65] S. Petrak,[65] B. N. Ratcliff,[65] S. H. Robertson,[65] A. Roodman,[65] A. A. Salnikov,[65] R. H. Schindler,[65] J. Schwiening,[65] G. Simi,[65] A. Snyder,[65] A. Soha,[65] J. Stelzer,[65] D. Su,[65] M. K. Sullivan,[65] H. A. Tanaka,[65] J. Va'vra,[65] S. R. Wagner,[65] M. Weaver,[65] A. J. R. Weinstein,[65] W. J. Wisniewski,[65] D. H. Wright,[65] C. C. Young,[65] P. R. Burchat,[66] T. I. Meyer,[66] C. Roat,[66] S. Ahmed,[67] J. A. Ernst,[67] W. Bugg,[68] M. Krishnamurthy,[68] S. M. Spanier,[68] R. Eckmann,[69] H. Kim,[69] J. L. Ritchie,[69] R. F. Schwitters,[69] J. M. Izen,[70] I. Kitayama,[70] X. C. Lou,[70] S. Ye,[70] F. Bianchi,[71] M. Bona,[71] F. Gallo,[71] D. Gamba,[71] C. Borean,[72] L. Bosisio,[72] G. Della Ricca,[72] S. Dittongo,[72] S. Grancagnolo,[72] L. Lanceri,[72] P. Poropat,[72,§] L. Vitale,[72] G. Vuagnin,[72] R. S. Panvini,[73] Sw. Banerjee,[74] C. M. Brown,[74] D. Fortin,[74] P. D. Jackson,[74] R. Kowalewski,[74] J. M. Roney,[74] H. R. Band,[75] S. Dasu,[75] M. Datta,[75] A. M. Eichenbaum,[75] H. Hu,[75] J. R. Johnson,[75] R. Liu,[75] F. Di Lodovico,[75] A. K. Mohapatra,[75] Y. Pan,[75] R. Prepost,[75] S. J. Sekula,[75] J. H. von Wimmersperg-Toeller,[75] J. Wu,[75] S. L. Wu,[75] Z. Yu,[75] and H. Neal[76]

(*BABAR* Collaboration)

[1]*Laboratoire de Physique des Particules, F-74941 Annecy-le-Vieux, France*
[2]*Università di Bari, Dipartimento di Fisica and INFN, I-70126 Bari, Italy*
[3]*Institute of High Energy Physics, Beijing 100039, China*
[4]*University of Bergen, Institute of Physics, N-5007 Bergen, Norway*
[5]*Lawrence Berkeley National Laboratory and University of California, Berkeley, California 94720, USA*
[6]*University of Birmingham, Birmingham B15 2TT, United Kingdom*
[7]*Ruhr Universität Bochum, Institut für Experimentalphysik 1, D-44780 Bochum, Germany*
[8]*University of Bristol, Bristol BS8 1TL, United Kingdom*
[9]*University of British Columbia, Vancouver, British Columbia, Canada V6T 1Z1*
[10]*Brunel University, Uxbridge, Middlesex UB8 3PH, United Kingdom*
[11]*Budker Institute of Nuclear Physics, Novosibirsk 630090, Russia*
[12]*University of California at Irvine, Irvine, California 92697, USA*
[13]*University of California at Los Angeles, Los Angeles, California 90024, USA*
[14]*University of California at San Diego, La Jolla, California 92093, USA*
[15]*University of California at Santa Barbara, Santa Barbara, California 93106, USA*
[16]*University of California at Santa Cruz, Institute for Particle Physics, Santa Cruz, California 95064, USA*
[17]*California Institute of Technology, Pasadena, California 91125, USA*
[18]*University of Cincinnati, Cincinnati, Ohio 45221, USA*
[19]*University of Colorado, Boulder, Colorado 80309, USA*
[20]*Colorado State University, Fort Collins, Colorado 80523, USA*
[21]*Technische Universität Dresden, Institut für Kern-und Teilchenphysik, D-01062 Dresden, Germany*
[22]*Ecole Polytechnique, LLR, F-91128 Palaiseau, France*
[23]*University of Edinburgh, Edinburgh EH9 3JZ, United Kingdom*
[24]*Università di Ferrara, Dipartimento di Fisica and INFN, I-44100 Ferrara, Italy*
[25]*Florida A&M University, Tallahassee, Florida 32307, USA*
[26]*Laboratori Nazionali di Frascati dell'INFN, I-00044 Frascati, Italy*
[27]*Università di Genova, Dipartimento di Fisica and INFN, I-16146 Genova, Italy*
[28]*Harvard University, Cambridge, Massachusetts 02138, USA*
[29]*Imperial College London, London SW7 2BW, United Kingdom*
[30]*University of Iowa, Iowa City, Iowa 52242, USA*
[31]*Iowa State University, Ames, Iowa 50011-3160, USA*
[32]*Laboratoire de l'Accélérateur Linéaire, F-91898 Orsay, France*

[33]*Lawrence Livermore National Laboratory, Livermore, California 94550, USA*
[34]*University of Liverpool, Liverpool L69 3BX, United Kingdom*
[35]*Queen Mary, University of London, E1 4NS, United Kingdom*
[36]*University of London, Royal Holloway and Bedford New College, Egham, Surrey TW20 0EX, United Kingdom*
[37]*University of Louisville, Louisville, Kentucky 40292, USA*
[38]*University of Manchester, Manchester M13 9PL, United Kingdom*
[39]*University of Maryland, College Park, Maryland 20742, USA*
[40]*University of Massachusetts, Amherst, Massachusetts 01003, USA*
[41]*Massachusetts Institute of Technology, Laboratory for Nuclear Science, Cambridge, Massachusetts 02139, USA*
[42]*McGill University, Montréal, Quebec, Canada H3A 2T8*
[43]*Università di Milano, Dipartimento di Fisica and INFN, I-20133 Milano, Italy*
[44]*University of Mississippi, University, Mississippi 38677, USA*
[45]*Université de Montréal, Laboratoire René J. A. Lévesque, Montréal, Quebec, Canada H3C 3J7*
[46]*Mount Holyoke College, South Hadley, Massachusetts 01075, USA*
[47]*Università di Napoli Federico II, Dipartimento di Scienze Fisiche and INFN, I-80126, Napoli, Italy*
[48]*NIKHEF, National Institute for Nuclear Physics and High Energy Physics, NL-1009 DB Amsterdam, The Netherlands*
[49]*University of Notre Dame, Notre Dame, Indiana 46556, USA*
[50]*Oak Ridge National Laboraotry, Oak Ridge, Tennessee 37831, USA*
[51]*The Ohio State University, Columbus, Ohio 43210, USA*
[52]*University of Oregon, Eugene, Oregon 97403, USA*
[53]*Università di Padova, Dipartimento di Fisica and INFN, I-35131 Padova, Italy*
[54]*Universités Paris VI et VII, Lab de Physique Nucléaire H. E., F-75252 Paris, France*
[55]*Università di Pavia, Dipartimento di Elettronica and INFN, I-27100 Pavia, Italy*
[56]*University of Pennsylvania, Philadelphia, Pennsylvania 19104, USA*
[57]*Università di Pisa, Dipartimento di Fisica, Scuola Normale Superiore and INFN, I-56127 Pisa, Italy*
[58]*Prairie View A&M University, Prairie View, Texas 77446, USA*
[59]*Princeton University, Princeton, New Jersey 08544, USA*
[60]*Università di Roma La Sapienza, Dipartimento di Fisica and INFN, I-00185, Roma, Italy*
[61]*Universität Rostock, D-18051 Rostock, Germany*
[62]*Rutherford Appleton Laboratory, Chilton, Didcot, Oxon, OX11 0QX, United Kingdom*
[63]*DSM/Dapnia, CEA/Saclay, F-91191 Gif-sur-Yvette, France*
[64]*University of South Carolina, Columbia, South Carolina 29208, USA*
[65]*Stanford Linear Accelerator Center, Stanford, California 94309, USA*
[66]*Stanford University, Stanford, California 94305-4060, USA*
[67]*State University of New York, Albany, New York 12222, USA*
[68]*University of Tennessee, Knoxville, Tennessee 37996, USA*
[69]*University of Texas at Austin, Austin, Texas 78712, USA*
[70]*University of Texas at Dallas, Richardson, Texas 75083, USA*
[71]*Università di Torino, Dipartimento di Fisica Sperimentale and INFN, I-10125 Torino, Italy*
[72]*Università di Trieste, Dipartimento di Fisica and INFN, I-34127 Trieste, Italy*
[73]*Vanderbilt University, Nashville, Tennessee 37235, USA*
[74]*University of Victoria, Victoria, British Columbia, Canada V8W 3P6*
[75]*University of Wisconsin, Madison, Wisconsin 53706, USA*
[76]*Yale University, New Haven, Connecticut 06511, USA*

(Received 17 June 2003; published 18 March 2004)

A search of the exclusive radiative decays $B \to \rho(770)\gamma$ and $B^0 \to \omega(782)\gamma$ is performed on a sample of about 84×10^6 $B\overline{B}$ events collected by the *BABAR* detector at the SLAC PEP-II asymmetric-energy e^+e^- storage ring. No significant signal is seen in any of the channels. We set upper limits on the branching fractions $\mathcal{B}$ of $\mathcal{B}(B^0 \to \rho^0\gamma) < 1.2 \times 10^{-6}$, $\mathcal{B}(B^+ \to \rho^+\gamma) < 2.1 \times 10^{-6}$, and $\mathcal{B}(B^0 \to \omega\gamma) < 1.0 \times 10^{-6}$ at 90% confidence level (C.L.). Using the assumption that $\Gamma(B \to \rho\gamma) = \Gamma(B^+ \to \rho^+\gamma) = 2 \times \Gamma(B^0 \to \rho^0\gamma)$, we find the combined limit $\mathcal{B}(B \to \rho\gamma) < 1.9 \times 10^{-6}$, corresponding to $\mathcal{B}(B \to \rho\gamma)/\mathcal{B}(B \to K^*\gamma) < 0.047$ at 90% C.L.

DOI: 10.1103/PhysRevLett.92.111801 PACS numbers: 12.15.Hh, 11.30.Er, 13.25.Hw

Within the standard model (SM), the decays $B \to \rho\gamma$ and $B^0 \to \omega\gamma$ proceed primarily through an underlying $b \to d\gamma$ electromagnetic "penguin" diagram that contains a top quark in the loop [1]. These processes are analogous to the $B \to K^*\gamma$ process mediated by the $b \to s\gamma$ transition, but with the final-state s quark replaced by a d quark, and the relevant element of the Cabibbo-Kobayashi-Maskawa (CKM) matrix changed from V_{ts} to V_{td}. There may also be contributions resulting from physics beyond the SM, such as supersymmetry [2]. Recent calculations of the branching fraction in the SM indicate a range $\mathcal{B}(B^+ \to \rho^+\gamma) = (0.9 - 1.5) \times 10^{-6}$

[3,4]. The range is due both to uncertainties in the value of V_{td} and to uncertainties in the calculation of the relevant hadronic form factors. The rates for $B^0 \to \rho^0\gamma$, $B^+ \to \rho^+\gamma$, and $B^0 \to \omega\gamma$ are related by the quark model, such that we expect $\Gamma(B^+ \to \rho^+\gamma) \approx 2 \times \Gamma(B^0 \to \rho^0\gamma) \approx 2 \times \Gamma(B^0 \to \omega\gamma)$. Previous searches [5] have found no evidence for these decays, nor any other $b \to d\gamma$ processes.

The analysis uses data collected by the *BABAR* detector [6] at the SLAC PEP-II asymmetric-energy e^+e^- storage ring [7]. The data sample consists of $(84.4 \pm 0.9) \times 10^6$ $B\overline{B}$ events corresponding to 78 fb^{-1} on the $\Upsilon(4S)$ resonance ("on resonance"), and 9.6 fb^{-1} recorded 40 MeV below the $\Upsilon(4S)$ resonance ("off resonance").

The *BABAR* detector consists of five subdetectors. Charged-particle trajectories are measured in both a five-layer silicon vertex tracker (SVT) and a 40-layer drift chamber (DCH) in a 1.5-T solenoidal magnetic field. Photons and electrons are detected in a CsI(Tl) electromagnetic calorimeter (EMC), with photon energy resolution $\sigma_E/E = 0.023(E/\text{GeV})^{-1/4} \oplus 0.019$. A ring-imaging Cherenkov detector (DIRC) is used for charged-particle identification. The magnetic flux return is instrumented with resistive plate chambers to identify muons.

The decay $B \to \rho\gamma$ is reconstructed with $\rho^0 \to \pi^+\pi^-$ and $\rho^+ \to \pi^+\pi^0$, while $B^0 \to \omega\gamma$ is reconstructed with $\omega \to \pi^+\pi^-\pi^0$. Charge-conjugate channels are implied throughout this Letter. Background high-energy photons are produced primarily in continuum u, d, s, and c quark-antiquark events through $\pi^0/\eta \to \gamma\gamma$ decays or via initial-state radiation. The reconstruction uses quantities both in the laboratory and $\Upsilon(4S)$ center-of-mass frames, where the latter are denoted by an asterisk.

The primary photon in the B decay is identified as an energy deposition in the EMC. The deposition must meet a number of criteria (described in detail in our Letter [8] on $B \to K^*\gamma$) that reduce background from charged particles, hadronic showers, and π^0 and η decays.

As in Ref. [8], the charged tracks used in identifying the ρ/ω meson are well-measured tracks with a momentum transverse to the beam direction greater than 0.1 GeV/c. A charged pion selection based on dE/dx measurements in the SVT and DCH and on Cherenkov photons reconstructed in the DIRC is used to reduce backgrounds from the $b \to s\gamma$ processes by rejecting charged kaons (e.g., K^+ from $B^0 \to K^{*0}\gamma$). Figure 1(a) shows the particle identification performance measured with a control sample of $D^{*+} \to D^0(\to K^-\pi^+)\pi^+$ decays.

Neutral pion candidates are identified using two photon candidates reconstructed in the calorimeter, each with energy greater than 50 MeV. The invariant mass of the pair is required to satisfy $115 < m_{\gamma\gamma} < 150$ MeV/c^2, which removes pairs whose invariant mass differs from the true m_{π^0} by more than about 3 times the experimental resolution. A kinematic fit with $m_{\gamma\gamma}$ constrained to m_{π^0} is used to improve the momentum resolution.

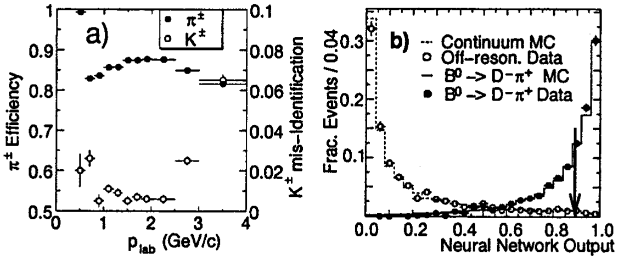

FIG. 1. (a) Pion efficiency and kaon misidentification of the charged pion selection for $0.4\ \text{GeV}/c < p_{\text{lab}} < 4.0\ \text{GeV}/c$, where p_{lab} is the track momentum in the laboratory frame. (b) $B^0 \to \rho^0\gamma$ neural-network output for MC-simulated events with comparison to data control samples. Events with neural-network output greater than 0.9 are selected, as indicated.

A ρ^0 candidate is reconstructed by selecting two identified pions that have opposite charge and a common vertex. The ρ^+ candidates are obtained by pairing π^0 candidates with an identified charged pion. We select ρ candidates with invariant mass $m_{\pi\pi}$ within 250 MeV/c^2 of $m_\rho = 770$ MeV/c^2 [9] and momentum $2.3 < p^*_{\pi\pi} < 2.85$ GeV/c. The ω candidates are reconstructed from combinations of oppositely charged identified pions with a common vertex and π^0 candidates with invariant mass $m_{\pi^+\pi^-\pi^0}$ within 23 MeV/c^2 of $m_\omega = 783$ MeV/c^2 [9] and momentum $2.4 < p^*_{\pi^+\pi^-\pi^0} < 2.8$ GeV/c. The $m_{\pi^+\pi^-\pi^0}$ resolution is slightly poorer in data than in Monte Carlo (MC) simulation. The resulting change in signal efficiency of the $m_{\pi^+\pi^-\pi^0}$ selection is accounted for as a systematic error in the signal efficiency.

The photon and ρ/ω meson candidates are combined to form the B meson candidates. We define $\Delta E^* \equiv E^*_B - E^*_{\text{beam}}$, where E^*_{beam} is the energy of each beam and $E^*_B = E^*_\gamma + E^*_{\rho/\omega}$ is the energy of the B meson candidate. The signal candidates are centered at $\Delta E^* = 0$ with resolution of about 50 MeV and a tail towards negative ΔE^* due to the asymmetric-energy response of the EMC. We also define the beam-energy-substituted mass $m_{\text{ES}} \equiv \sqrt{E^{*2}_{\text{beam}} - p'^{*2}_B}$, where p'^*_B is the momentum of the B candidate modified by scaling the photon energy to make $E^*_\gamma + E^*_{\rho/\omega} - E^*_{\text{beam}} = 0$. This procedure reduces the tail in the signal m_{ES} distribution that results from the asymmetric calorimeter response. The signal candidates peak at $m_{\text{ES}} = m_B$ with a resolution of about 3 MeV/c^2, dominated by the beam-energy spread.

We consider candidates in the "fit region" $-0.3 < \Delta E^* < 0.3$ GeV and $5.20 < m_{\text{ES}} < 5.29$ GeV/c^2. For those events in which more than one B meson candidate satisfies all the cuts (8% of MC $B^0 \to \rho^0\gamma$ events), we select the candidate with the smallest value of $|\Delta E^*|$.

We construct a number of variables that distinguish the signal from the continuum $q\overline{q}$ background. As in Ref. [8], we calculate the thrust angle θ^*_T, the B-production angle θ^*_B, and the helicity angle θ_H. For $B^0 \to \omega\gamma$, θ_H is defined as the angle between the normal to the decay plane of the ω and the flight direction of the B meson, both computed in the ω rest frame. We also calculate several additional discriminating variables. The energy flow of the event excluding the B-meson daughters in 10° cones centered on the photon-candidate momentum provides discrimination between the jetlike continuum background and the more spherical signal events. For suppression of the initial-state radiation background, we consider R_2', the ratio of second- to zeroth-order Fox-Wolfram moments [10] in the frame recoiling from the photon momentum. We define the net flavor content as $\sum_i |N_i^+ - N_i^-|$, where $N_i^{\pm}$ are the number of $e^{\pm}$, $\mu^{\pm}$, $K^{\pm}$, and slow pions of each sign identified in the event [11]. On average, $B\overline{B}$ events have larger net flavor than continuum events. In the $B^0 \to \rho^0\gamma$ and $B^0 \to \omega\gamma$ analyses, we use the separation along the beam axis of the B-meson candidate vertex and that of the rest of the event. This variable is useful due to the finite B lifetime. In the $B^0 \to \omega\gamma$ analysis, we use the ω Dalitz angle θ_D, which is defined as the angle between the π^0 and the π^+ in the $\pi^+\pi^-$ rest frame [12]; $\cos\theta_D$ follows a $\sin^2\theta_D$ distribution for true ω decays, as opposed to the uniform distribution of combinatorial background.

The background-suppression variables are combined into one discriminating variable via a neural network, which responds nonlinearly to the input variables and exploits correlations between the variables [13]. A separate neural network is trained for each mode.

The output for the neural network trained for $B^0 \to \rho^0\gamma$ is shown in Fig. 1(b), where the MC simulation of the continuum background is compared with the off-resonance data, and the output for MC-simulated $B^0 \to D^-\pi^+$ decays is compared with $B^0 \to D^-\pi^+$ decays reconstructed in the on-resonance data. The latter comparison provides a cross-check of those input variables that depend on the properties of the other B meson in the event. This includes all of the variables except for θ_H and θ_D, which, for this check, are modeled using the signal distributions.

To suppress the continuum background, we make a selection on the neural-network output that is optimized for minimum statistical error as determined using MC samples of signal and background. The efficiency of this selection for the $B \to D\pi$ control sample differs slightly between the data and MC simulation. We account for this difference as a systematic error in the signal efficiency. For $B^+ \to \rho^+\gamma$, we also require $|\cos\theta_H| < 0.6$ to reject $B^+ \to \rho^+\pi^0$ events, which have a $\cos^2\theta_H$ distribution, as opposed to the expected $\sin^2\theta_H$ distribution of the signal process.

After applying the neural network, $\cos\theta_H$, and fit-region selection to the on-resonance data, 449 events remain in the $B^0 \to \rho^0\gamma$ data, 480 events for $B^+ \to \rho^+\gamma$, and 54 events for $B^0 \to \omega\gamma$. MC studies indicate that about 90% of the background in these samples comes from continuum events, and only about 10% from $B\overline{B}$.

For the signal extraction, we perform an unbinned extended maximum likelihood fit to the selected events. For $B \to \rho\gamma$, the fit uses m_{ES}, ΔE^*, and $m_{\pi\pi}$, whereas for $B^0 \to \omega\gamma$, only m_{ES} and ΔE^* are used. The measured variables are largely uncorrelated, even after the $p^*_{\pi\pi}$ (or $p^*_{\pi^+\pi^-\pi^0}$) cut, allowing the probability density function (PDF) to be constructed as a product of independent distributions for each variable. Since the $B\overline{B}$ backgrounds have PDFs that largely resemble continuum but are much smaller, the signal extraction uses only a continuum component to describe the background. Biases due to $B\overline{B}$ backgrounds are considered below. The signal m_{ES} and ΔE^* distributions are described by the "crystal ball" shape [14], with the exception of the m_{ES} distribution for $B^0 \to \rho^0\gamma$, where the Gaussian distribution is used. The relativistic Breit-Wigner line shape is used for the signal $m_{\pi\pi}$ distribution. The signal PDF parameters are obtained from MC simulation. The background m_{ES} and ΔE^* distributions are described by the ARGUS threshold function [15] and a second-order polynomial, respectively. The background $m_{\pi\pi}$ function is a sum of a Breit-Wigner component and a combinatorial component described by a first order polynomial. The background PDF parameters are determined in the fit, with the exception of the $m_{\pi\pi}$ resonant fraction, which is fixed to the value measured in off-resonance data.

The ΔE^* vs m_{ES} distributions of the selected $B \to \rho\gamma$ and $B^0 \to \omega\gamma$ candidates are shown in Fig. 2 and the fitted signal yields are shown in Table I. No significant signal is seen in any mode. The quality of the fit is checked by comparing the overall likelihood of the fit with values obtained from an ensemble of

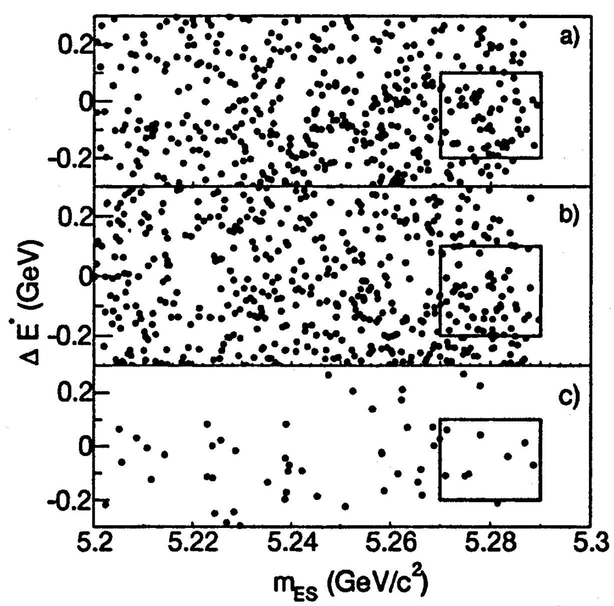

FIG. 2. ΔE^* vs m_{ES} fit regions for (a) $B^0 \to \rho^0\gamma$, (b) $B^+ \to \rho^+\gamma$, and (c) $B^0 \to \omega\gamma$ candidates. The boxes indicate the regions where signal events would appear: $-0.2 < \Delta E^* < 0.1$ GeV and $5.27 < m_{ES} < 5.29$ GeV$/c^2$. Assuming $\mathcal{B}(B^0 \to \rho^0\gamma) = \frac{1}{2}\mathcal{B}(B^+ \to \rho^+\gamma) = \mathcal{B}(B^0 \to \omega\gamma) = 10^{-6}$, we expect 9.9, 12.1, and 3.4 signal events in these regions, respectively.

TABLE I. The signal yields and errors obtained from the signal extraction fit, the ranges of observed biases from $B\overline{B}$ backgrounds, selection efficiencies (ϵ), and the inferred branching fractions ($\mathcal{B}$) for $B^0 \to \rho^0\gamma$, $B^+ \to \rho^+\gamma$, and $B^0 \to \omega\gamma$ in the on-resonance data sample. The "upper lim." is a 90% C.L. limit. The efficiencies include the partial branching fractions for the ρ/ω decays considered.

Mode	Yield (Events)	Bias (Events)	Upper lim. (Events)	ϵ (%)	$\mathcal{B}$ (10^{-6})
$B^0 \to \rho^0\gamma$	$4.8^{+5.7}_{-4.7}$	$[-0.5, 0.8]$	12.4	12.3	$0.4^{+0.6}_{-0.5}$
$B^+ \to \rho^+\gamma$	$6.2^{+7.2}_{-6.2}$	$[-0.1, 2.0]$	15.4	9.2	$0.7^{+0.9}_{-0.8}$
$B^0 \to \omega\gamma$	$0.1^{+2.7}_{-2.0}$	$[-0.3, 0.5]$	3.6	4.6	$0.0^{+0.7}_{-0.5}$

parametrized MC simulations and found to be within the range expected.

We consider three sources of systematic uncertainty in this analysis: the modeling of $B\overline{B}$ backgrounds, the signal reconstruction efficiency, and the fixed parameters of the PDFs used in the fit. The first of these is "additive" in that it could result in background adding to the fitted signal yields. The last two are "multiplicative" in that they affect the way a given signal is interpreted as a branching fraction.

The effect that $B\overline{B}$ backgrounds have on the fitted signal yields is studied with parametrized MC simulations of the $m_{\rm ES}$, ΔE^*, and $m_{\pi\pi}$ distributions. Possible correlations in the $m_{\rm ES}$-ΔE^* plane are modeled with two-dimensional distributions. Also, the rates of the dominant background modes are varied within wide ranges. For $b \to s\gamma$ (including $B \to K^*\gamma$), the normalization is varied between zero and twice the nominal value to conservatively account for uncertainties in kaon misidentification. For $B^+ \to \rho^+\pi^0$ decays the branching fraction is varied between zero and twice the expected rate of 2×10^{-5} [16]. Much lower branching fractions are expected for $B^0 \to \rho^0\pi^0$ and $B^0 \to \omega\pi^0$ [16], so these cause negligible backgrounds. The small biases in Table I confirm that the $B\overline{B}$ PDFs are similar to those of continuum background.

All signal-efficiency systematic uncertainties, except those related to the neural network and the ω mass, which are described above, are estimated in Ref. [8]. The largest uncertainties, which arise from the neural net efficiencies, are 5%, 5%, and 10% for $B^0 \to \rho^0\gamma$, $B^+ \to \rho^+\gamma$, and $B^0 \to \omega\gamma$, respectively. The π^0 efficiency also contributes a 5% uncertainty to $B^+ \to \rho^+\gamma$ and $B^0 \to \omega\gamma$.

The fixed parameters of the signal PDFs are studied in fits to data for the topologically and kinematically similar, but much more common, $B \to K^*\gamma$ decays: $B^0 \to K^{*0}\gamma$, $K^{*0} \to K^+\pi^-$ for $B^0 \to \rho^0\gamma$ and $B^+ \to K^{*+}\gamma$, $K^{*+} \to K^+\pi^0$ for $B^+ \to \rho^+\gamma$ and $B^0 \to \omega\gamma$. In these fits, the signal PDF parameters are allowed to float. The signal event yields are compared to those expected from the branching fractions measured in Ref. [8] and found to agree.

The statistical uncertainties of the PDF parameters, one of which is the background $m_{\pi\pi}$ resonant fraction, are used as ranges within which we vary the parameters of the $B \to (\rho/\omega)\gamma$ fits. The resulting variations in the fitted signal yield, which amount to 5% for $B^0 \to \rho^0\gamma$ and $B^0 \to \omega\gamma$ and 10% for $B^+ \to \rho^+\gamma$, are taken as systematic uncertainties. The total multiplicative systematic error, including the signal-efficiency uncertainty, is 8% for $B^0 \to \rho^0\gamma$ and 13% for $B^+ \to \rho^+\gamma$ and $B^0 \to \omega\gamma$.

We assume $\mathcal{B}(\Upsilon(4S) \to B^0\overline{B}^0) = \mathcal{B}(\Upsilon(4S) \to B^+B^-) = 0.5$. In calculating upper limits, we correct for bias from $B\overline{B}$ backgrounds by subtracting the smallest observed bias, which is found to be negative for all three modes, from the signal yield. We include the effects of the multiplicative systematic uncertainties by using an extension [17] of the method described in Ref. [18], wherein the systematic and staistical errors are convolved. The resulting 90% confidence level (C.L.) upper limits for the branching fractions are $\mathcal{B}(B^0 \to \rho^0\gamma) < 1.2 \times 10^{-6}$, $\mathcal{B}(B^+ \to \rho^+\gamma) < 2.1 \times 10^{-6}$, and $\mathcal{B}(B^0 \to \omega\gamma) < 1.0 \times 10^{-6}$. Although no significant signals are seen, Table I shows the measured $\mathcal{B}$ for each mode. For this calculation, we subtract a bias corresponding to the center of the allowed range, treat the half-width of the range as the systematic error, and add systematic and statistical errors in quadrature.

We also calculate a combined limit for the generic process $B \to \rho\gamma$ by assuming $\Gamma(B \to \rho\gamma) = \Gamma(B^+ \to \rho^+\gamma) = 2 \times \Gamma(B^0 \to \rho^0\gamma)$ and using the lifetime ratio $\tau_{B^+}/\tau_{B^0} = 1.083 \pm 0.017$ [9]. The resulting 90% C.L. upper limit is $\mathcal{B}(B \to \rho\gamma) < 1.9 \times 10^{-6}$. Using the measured value of $\mathcal{B}(B \to K^*\gamma)$ [8], this corresponds to a limit of $\mathcal{B}(B \to \rho\gamma)/\mathcal{B}(B \to K^*\gamma) < 0.047$.

This limit may be used to constrain the ratio of CKM elements $|V_{td}/V_{ts}|$ by means of the equation [4]:

$$\frac{\mathcal{B}(B \to \rho\gamma)}{\mathcal{B}(B \to K^*\gamma)} = \left|\frac{V_{td}}{V_{ts}}\right|^2 \left(\frac{1 - m_\rho^2/M_B^2}{1 - m_{K^*}^2/M_B^2}\right)^3 \zeta^2[1 + \Delta R],$$

where ζ describes the flavor-SU(3) breaking between ρ and K^*, and ΔR accounts for annihilation diagrams. ΔR is different for ρ^0 and ρ^+, but we do not take this into account here. Both ζ and ΔR must be taken from theory and there are several different [4,19] values published. As an example, we choose the values $\zeta = 0.76 \pm 0.10$ and $\Delta R = 0.0 \pm 0.2$. We adjust both parameters down by one σ and find the limit $|V_{td}/V_{ts}| < 0.34$ at 90% C.L.

In conclusion, we have found no evidence for the exclusive $b \to d\gamma$ transitions $B \to \rho\gamma$ and $B^0 \to \omega\gamma$ in $(84.4 \pm 0.9) \times 10^6$ $B\overline{B}$ decays studied with the BABAR detector. The 90% C.L. upper limits on the branching fractions are significantly lower than previous values and start to restrict the range indicated by SM predictions [3,4].

We are grateful for the excellent luminosity and machine conditions provided by our PEP-II colleagues and for the substantial dedicated effort from the computing organizations that support *BaBar*. The collaborating institutions thank SLAC for its support and kind hospitality. This work is supported by DOE and NSF (USA), NSERC (Canada), IHEP (China), CEA and CNRS-IN2P3 (France), BMBF and DFG (Germany), INFN (Italy), FOM (The Netherlands), NFR (Norway), MIST (Russia), and PPARC (United Kingdom). Individuals have received support from the A. P. Sloan Foundation, Research Corporation, and Alexander von Humboldt Foundation.

*Also with Università di Perugia, Perugia, Italy.
†Also with Università della Basilicata, Potenza, Italy.
‡Also with IFIC, Instituto de Física Corpuscular, CSIC-Universidad de Valencia, Valencia, Spain.
§Deceased.

[1] For a review, see K. Lingel, T. Skwarnicki, and J. G. Smith, Annu. Rev. Nucl. Part. Sci. **48**, 253 (1998).
[2] See, for example, S. Bertolini, F. Borzumati, and A. Masiero, Nucl. Phys. **B294**, 321 (1987); H. Baer and M. Brhlik, Phys. Rev. D **55**, 3201 (1997); J. Hewett and J. Wells, Phys. Rev. D **55**, 5549 (1997); M. Carena *et al.*, Phys. Lett. B **499**, 141 (2001).
[3] S.W. Bosch and G. Buchalla, Nucl. Phys. **B621**, 459 (2002).
[4] A. Ali and Ya. Parkhomenko, Eur. Phys. J. C **23**, 89 (2002).
[5] CLEO Collaboration, T. E. Coan *et al.*, Phys. Rev. Lett. **84**, 5283 (2000); Belle Collaboration, Y. Ushiroda *et al.*, hep-ex/0104045.
[6] BABAR Collaboration, B. Aubert *et al.*, Nucl. Instrum. Methods Phys. Res., Sect. A **479**, 1 (2002).
[7] PEP-II Conceptual Design Report, SLAC Report No. SLAC-0418, 1993.
[8] BABAR Collaboration, B. Aubert *et al.*, Phys. Rev. Lett. **88**, 101805 (2002).
[9] Particle Data Group, K. Hagiwara *et al.*, Phys. Rev. D **66**, 010001 (2002).
[10] G. C. Fox and S. Wolfram, Nucl. Phys. **B149**, 413 (1979).
[11] BABAR Collaboration, B. Aubert *et al.*, Phys. Rev. D **66**, 032003 (2002).
[12] H. Muirhead, *Notes on Elementary Particle Physics* (Pergamon Press, Oxford, 1971), p. 135.
[13] We use the Stuttgart Neural-Network Simulator (http://www-ra.informatik.uni-tuebingen.de/SNNS) to train a neural net with one hidden layer of ten nodes.
[14] The crystal ball (CB) line shape is a modified Gaussian distribution with a transition to a tail function on the low side: $f_{\rm CB} = \exp(-\frac{(x-\mu)^2}{2\sigma^2})$ for $\frac{x-\mu}{\sigma} > \alpha$ and $A \times [B - (\frac{x-\mu}{\sigma})]^{-n}$ for $\frac{x-\mu}{\sigma} < \alpha$, where $A \equiv (\frac{n}{|\alpha|})^n \exp(-\frac{1}{2}\alpha^2)$ and $B \equiv \frac{n}{|\alpha|} - |\alpha|$ are defined such as to maintain continuity of the function and its first derivative.
[15] We use the distribution $x\sqrt{1-x^2} \times \exp[\zeta(1-x^2)]$, where $x = m_{\rm ES}/E^*_{\rm beam}$, to describe the background $m_{\rm ES}$ distribution. H. Albrecht *et al.*, Z. Phys. C **48**, 543 (1990).
[16] Y.-H. Chen *et al.*, Phys. Rev. D **60**, 094014 (1999).
[17] M. R. Convery, SLAC Report No. SLAC-TN-03-001, 2003.
[18] R. Cousins and V. Highland, Nucl. Instrum. Methods Phys. Res., Sect. A **320**, 331 (1992).
[19] B. Grinstein and D. Pirjol, Phys. Rev. D **62**, 093002 (2000).